Fluorescence-Force Spectroscopy Maps Two-Dimensional Reaction Landscape of the Holliday Junction

Sungchul Hohng, *et al.*

Science **318**, 279 (2007);
DOI: 10.1126/science.1146113

21. S. J. Deminoff, S. C. Howard, A. Hester, S. Warner, P. K. Herman, *Genetics* **173**, 1909 (2006).
22. H. M. Berman *et al.*, *Proc. Natl. Acad. Sci. U.S.A.* **102**, 45 (2005).
23. H. Rehmann, A. Wittinghofer, J. L. Bos, *Nat. Rev. Mol. Cell Biol.* **8**, 63 (2007).
24. L. J. Huang, S. S. Taylor, *J. Biol. Chem.* **273**, 26739 (1998).
25. Abbreviations for amino acid residues: A, Ala; C, Cys; D, Asp; E, Glu; F, Phe; G, Gly; H, His; I, Ile; K, Lys; L, Leu; M, Met; N, Asn; P, Pro; Q, Gln; R, Arg; S, Ser; T, Thr; V, Val; W, Trp; Y, Tyr.
26. We thank the Advanced Light Source for assistance in data collection, E. Radzio-Andzelm for assistance in preparation of the figures, and M. Deal for purification of the C subunit. Supported by NIH grant GM34921 (S.S.T.) and NIH training grant T32-CA009524 (S.H.J.B.). The coordinate and structure factor are deposited with the Protein Data Bank (PDB accession code 2QVS).

Supporting Online Material
www.sciencemag.org/cgi/content/full/318/5848/274/DC1
Materials and Methods
Figs. S1 to S6
Tables S1 and S2
References

13 June 2007; accepted 11 September 2007
10.1126/science.1146447

Fluorescence-Force Spectroscopy Maps Two-Dimensional Reaction Landscape of the Holliday Junction

Sungchul Hohng,[1,2]* Ruobo Zhou,[1] Michelle K. Nahas,[1] Jin Yu,[1,4] Klaus Schulten,[1,3,4] David M. J. Lilley,[5] Taekjip Ha[1,2,3,4]†

Despite the recent advances in single-molecule manipulation techniques, purely mechanical approaches cannot detect subtle conformational changes in the biologically important regime of weak forces. We developed a hybrid scheme combining force and fluorescence that allowed us to examine the effect of subpiconewton forces on the nanometer scale motion of the Holliday junction (HJ) at 100-hertz bandwidth. The HJ is an exquisitely sensitive force sensor whose force response is amplified with an increase in its arm lengths, demonstrating a lever-arm effect at the nanometer-length scale. Mechanical interrogation of the HJ in three different directions helped elucidate the structures of the transient species populated during its conformational changes. This method of mapping two-dimensional reaction landscapes at low forces is readily applicable to other nucleic acid systems and their interactions with proteins and enzymes.

Many biological processes are dependent on tension. In recent years, single-molecule force measurements have shown directly that biochemical reactions can be influenced by applied force (*1*). Yet, purely mechanical tools cannot detect small-scale conformational changes unless strong and persistent force is applied. At weak forces, the flexible tether connecting the mechanical probe to the biological molecule is not stretched enough to transmit small movements. This is unfortunate because weak and transient forces are likely more prevalent in vivo, but the experimental limitations confine single-molecule mechanical studies to examining the effect of relatively large forces. We aimed to study the effect of weak external forces on the biomolecular conformational dynamics by combining single-molecule fluorescence resonance energy transfer (smFRET) (*2*–*4*) with manipulation using optical trap (*5*). smFRET has high spatial resolution [≤ 5 Å (*6*, *7*)] and can be measured at arbitrarily low forces. Previous attempts to combine FRET and optical trap using the DNA hairpin as a model system (*8*, *9*) did not reveal new information because the hairpin unzips at high forces (~15 pN), a regime that had been extensively investigated using force-based techniques (*10*, *11*). Here, we report an approach to detect nanometer-scale motion at sub-pN forces. We used the approach to gain insight into the reaction landscape of the Holliday junction (HJ) by gently stretching it along different directions.

The HJ is a four-stranded DNA structure that forms as an intermediate during recombination (*12*). To understand the mechanisms of cellular enzymes that function with the HJ, a detailed description of the static and dynamic structural properties of the HJ itself is needed. In the absence of added ions, the HJ adopts an open structure, where the four helical arms point toward the corners of a square (*13*, *14*) (Fig. 1A). In the presence of physiological concentrations of magnesium ions, the HJ becomes more compact by pairwise coaxial stacking of helical arms into a right-handed antiparallel stacked-X structure (*13*–*15*). There are two ways of forming this stacked structure that depend upon the choice of helical stacking partners (*iso*I and *iso*II) (Fig. 1B). For these studies, we have chosen a sequence with nearly equal population of stacking conformers *iso*I and *iso*II (*16*) (*17*) (fig. S1). smFRET studies showed that an HJ continually switches between the two stacking conformations (*18*). At present, there is no structural information on the transient species populated during these conformational changes.

To investigate the nature of such transient HJ structures and to understand how HJ conformational properties could depend on physiologically relevant forces, we built a hybrid instrument that combines smFRET with optical trapping via a long linker (bacteriophage λ DNA) (*17*). The trapping and fluorescence excitation beams in our confocal microscope are spatially separated (minimum 13 μm) (Fig. 1C), such that fluorescence and force processes can operate without mutual interference. The long linker acts as a loose spring that dampens the random forces generated by Brownian motion of the trapped bead and reduces force variations due to the nanometer-scale conformational change of the HJ. The effective stiffness of the λ DNA at 2 pN of force is about 0.002 pN/nm, such that a 5-nm movement of the HJ causes negligible force fluctuations (~0.01 pN) at the trapped bead. Therefore, the measurements can be performed under effectively constant force without the need for active force clamping. The relaxation time scales of the λ DNA under tension are faster than the time scale of conformational fluctuations we investigated (*19*). The trapping beam (1064 nm) was fixed along the optical axis of the microscope, and force was applied by moving the surface-tethered HJ using a piezoelectric sample scanner. The confocal excitation beam (532 nm) was programmed to follow the HJ using a piezo-controlled mirror to maintain uniform excitation and detection efficiencies regardless of the specimen location (and therefore force) (*17*).

To determine comprehensively the force response of the HJ, we used the following four constructs (Fig. 1A). The four helices composing the HJ are named B (red), H (green), R (dark gray), and X (gray). Helix R was labeled at its 5′ terminus with biotin for surface immobilization, and helices X, H, or B were extended by a 12-nt single-stranded DNA 5′ overhang to permit annealing to a cohesive end of λ DNA (named junctions *XR*, *HR*, and *BR*, respectively). The other end of the λ DNA was attached to a bead via digoxigenin/anti-digoxigenin coupling in order to pull on the DNA using optical tweezers in three different directions, between the X and R arms for junction *XR*, and so on. Junctions *XR* and *XR*-long differ in the length of the X and R arms [11 base pairs (bp) versus 21 bp]. Cy3 (FRET donor) was attached to the end of helix H, and Cy5 (acceptor) to the end of helix B. For

[1]Department of Physics, University of Illinois at Urbana-Champaign, Urbana, IL 61801, USA. [2]Howard Hughes Medical Institute, Urbana, IL 61801, USA. [3]Center for Biophysics and Computational Biology, University of Illinois at Urbana-Champaign, Urbana, IL 61801, USA. [4]Beckman Institute, University of Illinois at Urbana-Champaign, Urbana, IL 61801, USA. [5]Cancer Research UK Nucleic Acid Structure Research Group, MSI/WTB Complex, University of Dundee, Dundee DD1 5EH, UK.
*Present address: Department of Physics and Astronomy, Seoul National University, Seoul 151-742, Korea.
†To whom correspondence should be addressed. E-mail: tjha@uiuc.edu

junctions *XR* and *XR*-long, the stretching force should favor *iso*I (low FRET), in which there is a larger separation between the two tether points, over *iso*II (high FRET) (Fig. 1D). Indeed, single-molecule FRET histograms as a function of force show that the low FRET state is significantly favored at forces exceeding 0.5 and 1.0 pN for junctions *XR*-long and *XR*, respectively (Fig. 1, E and F). Likewise, *iso*II (high FRET) would be favored at high forces for junction *HR*. In contrast, the two tether points would have similar distances for *iso*I and *iso*II in the case of junction *BR*, and force-induced bias should be minimal.

Figure 2A shows smFRET time traces at five different forces (gray lines, 10 s duration each, with 10 ms integration time) obtained from a single molecule of junction *XR*. Enhanced photostability by means of the use of Trolox (*20*) allowed us to obtain one to five cycles of force data from a single molecule before photobleaching, corresponding to observation over 50 to 250 s. Idealized FRET trajectories generated by hidden Markov modeling (red lines) (*21*) are also shown. At the lowest force (0.3 pN), the junction switches between the high and low FRET states with similar populations. As the force exceeds 1 pN, the dynamics become clearly biased to the low FRET state. Figure 2B shows the transition rates determined from hidden Markov modeling as a function of force. The transition rate k_f for the forward reaction from the low FRET state (*iso*I) to the high FRET state (*iso*II) decreases with increasing force (blue), whereas the transition rate for the backward reaction k_b (*iso*II to *iso*I) increases with force (red) as expected. Both changes were linear in the log-linear scale but, interestingly, k_f had twice the slope of k_b. If the reaction is viewed as possessing a single transition state, the slope reflects the distance to the transition state (*1*). Therefore, the transition state lies closer to *iso*II than to *iso*I when force is applied by the *XR* vector. Averaged over five molecules, the distance from *iso*II to the transition state ($\Delta x_b^{\ddagger}$) is 1.5 ± 0.3 nm, and the distance from *iso*I to the transition state ($\Delta x_f^{\ddagger}$) is 2.9 ± 0.6 nm (Table 1).

We next studied junction *HR*, where the λ DNA tether has been transferred from the X to the H arm. In this construct, the force is expected to bias the HJ to the high-FRET *iso*II state, and indeed this was the result (Fig. 2C). k_b decreased and k_f increased with stronger forces, but with a slope twice as high for k_b as for k_f (Fig. 2D). Averaged over five molecules, $\Delta x_b^{\ddagger}$=2.4 ± 0.5 nm and $\Delta x_f^{\ddagger}$ = 1.3 ± 0.3 nm. In both junctions, ($\Delta x_b^{\ddagger}$ + $\Delta x_f^{\ddagger}$) is equal to the distance between *iso*I and *iso*II, Δx_{eq}, calculated from equilibrium population versus force data (Table 1). Therefore, the distances between the ends of the pulled arms, d_{XR} for junction *XR* and d_{HR} for junction *HR*, are suitable reaction coordinates spanning the complete trajectory from *iso*I to *iso*II (Fig. 3A).

In one pulling direction represented by d_{XR}, the transition state lies closer to *iso*II (Fig. 3A,

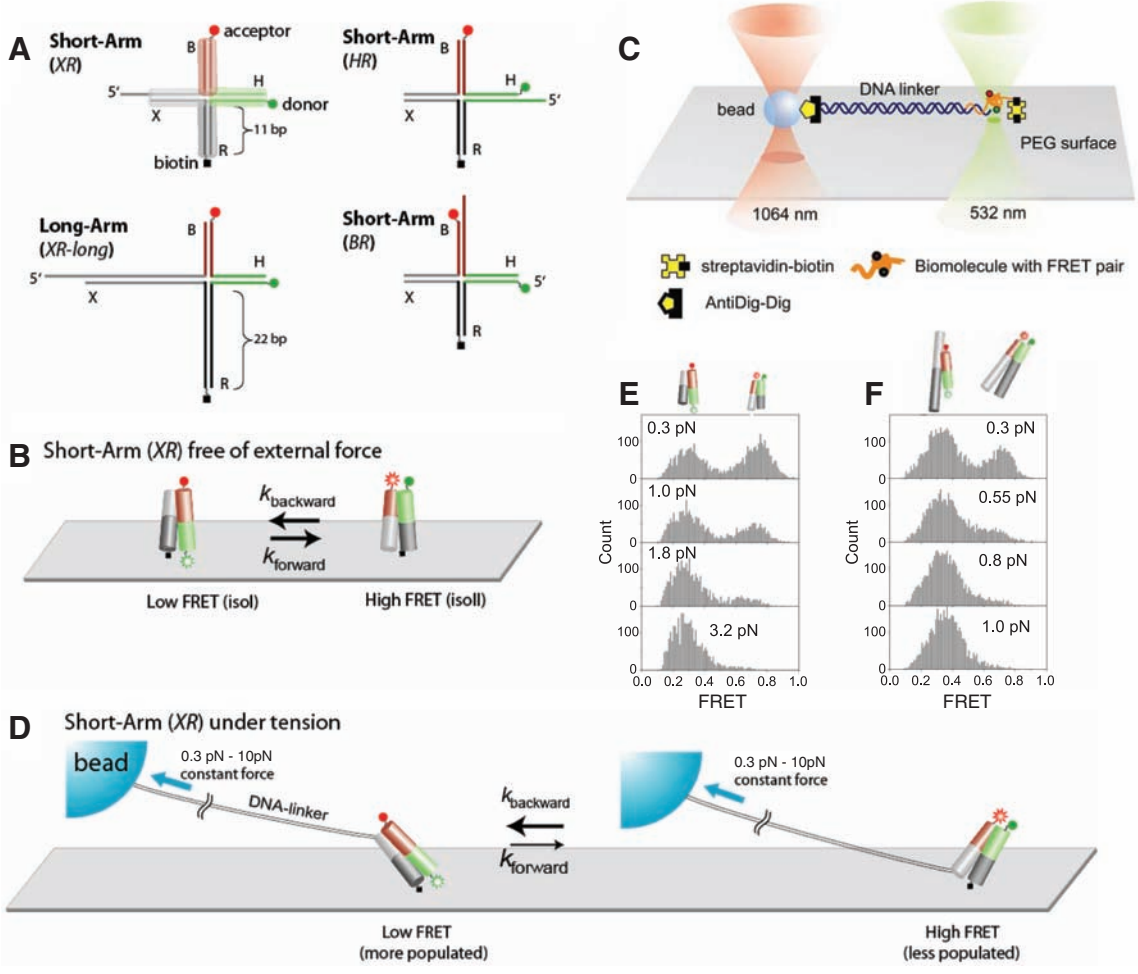

Fig. 1. Holliday junction constructs and experimental scheme. (**A**) The HJ species studied. Junction *XR* comprises four arms of 11 bp, termed B (red), H (green), R (dark gray), and X (gray). Cy3 and Cy5 fluorophores are terminally attached to H and B arms, respectively, and the molecule is tethered to the surface through biotin attached to the end of the R arm. Stretching force is applied through the λ DNA linker hybridized to the X arm. In junction *XR*-long, the lengths of arms R and X are increased to 21 bp. In junction *HR*, the λ DNA linker is hybridized to the H arm. In junctions *HR* and *BR*, the λ DNA linker is hybridized to the H and B arms, respectively. (**B**) Junction *XR* is known to alternate between two different stacking conformers, *iso*I (low FRET) and *iso*II (high FRET), with similar populations in both states. (**C**) A surface-immobilized biomolecule with FRET labeling is connected to a trapped bead by a long DNA linker. The linker DNA spatially separates the confocal beam (532 nm) from the trapping beam (1064 nm), such that enhanced photobleaching and an overwhelming background signal induced by the intense trapping laser are avoided. To apply force, the surface-immobilized molecule was moved relative to the trapped bead. The confocal beam was programmed to follow the motion of the molecule using the mapping generated between sample scanning and beam scanning (fig. S6). (**D**) Force is expected to bias the junction *XR* to *iso*I, which possesses a larger separation between the two tether points than *iso*II. (**E**) FRET histograms of a single-junction *XR* as a function of force. (**F**) FRET histograms of a single-junction *XR*-long as a function of force.

middle panel), whereas for the other pulling direction along d_{HR}, the transition state more closely resembles *iso*I (Fig. 3A, bottom panel). These two transition states cannot represent a single structure because then both d_{XR} and d_{HR} must be relatively small, and by symmetry so must be d_{XB} and d_{HB}. Such a structure would have all four helices in the same hemisphere relative to the junction core, which is highly unlikely considering the symmetry of the HJ. Instead, we favor a model in which there are at least two different transition states, *ts*I and *ts*II, equal in energy but corresponding to different values of d_{XR} (or d_{HR}), such that force would elevate one of them into the single highest energy barrier by the tilting of the energy landscape (Fig. 3A).

The data presented so far show that the distance change upon stacking conformer transitions is about 4 nm. Because thermal energy is about 4 pN nm, a force on the order of 1 pN would consequently change the equilibrium between the two states by a factor of two or three. Such small-scale conformational fluctuations at these low forces are probably impossible to detect

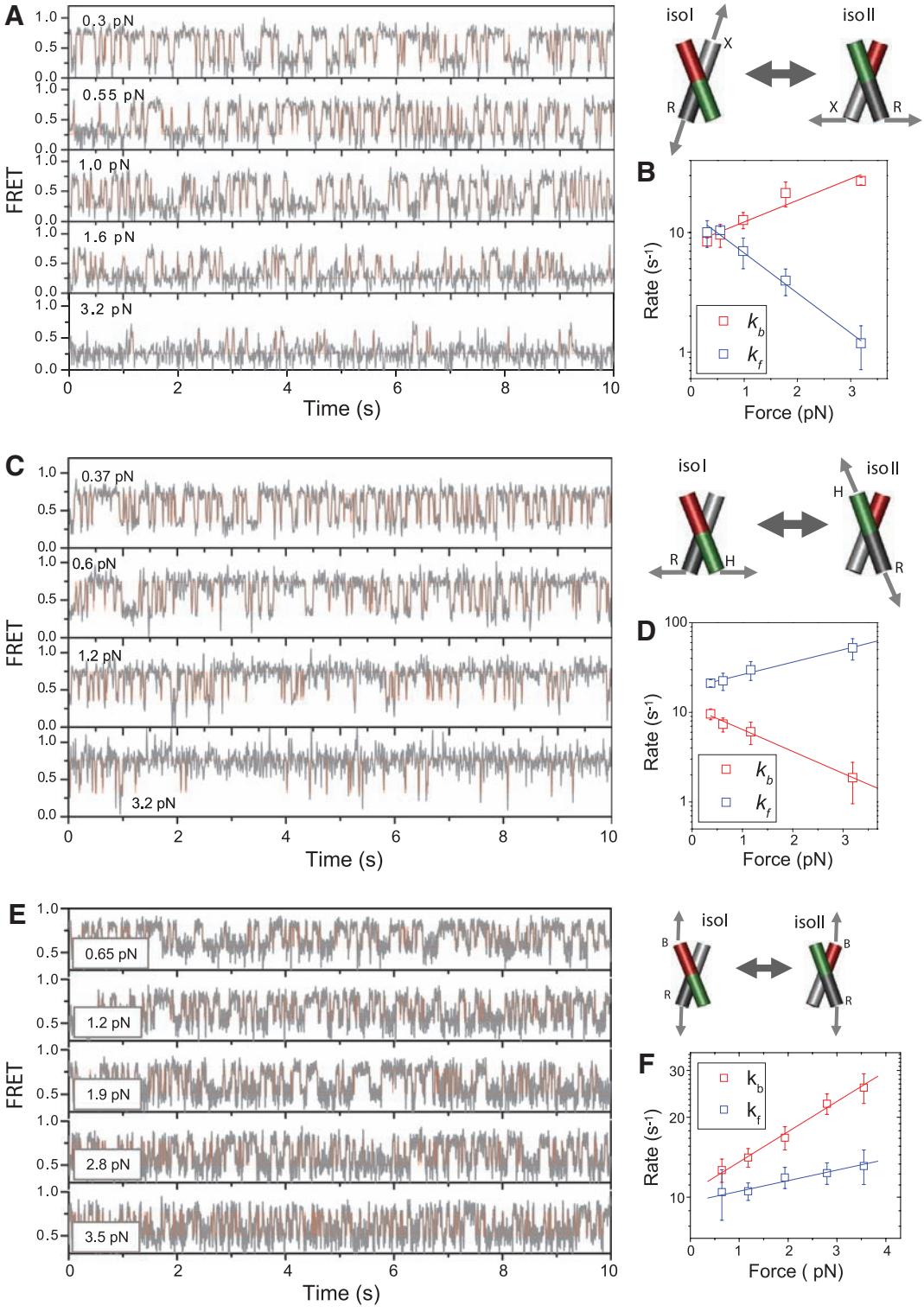

Fig. 2. Conformer exchange dynamics of the HJ as a function of applied force. (**A**) FRET time traces (gray lines) of a single-junction *XR* molecule at different forces. FRET efficiency is approximated by the acceptor intensity divided by the sum of the donor and acceptor intensities. Red lines are the most likely FRET trajectories generated by hidden Markov modeling. The imposed force (indicated on the top left of each plot) increases top to bottom. (**B**) Log-linear plot of rate constants of conformer exchange as a function of force. Rates of transition from states *iso*II to *iso*I (k_b, red) and *iso*I to *iso*II (k_f, blue) are differentiated by color. Error bars represent SDs obtained from repeated measurements of the same molecule. From linear fitting, we found that the transition state is closer to *iso*II (1.8 nm) than to *iso*I (3.3 nm). (**C**) Same as (A) but for a single-junction *HR* molecule. (**D**) Same as (B) but for a single-junction *HR* molecule. (**E**) Same as (A) and (C) but for a single-junction *BR* molecule. (**F**) Same as (B) and (D) but for a single-junction *BR* molecule.

in a purely mechanical measurement, especially at our time resolution (10 ms).

What determines the force sensitivity of the junction? Is it an intrinsic property of the junction core or is it dependent on the length of helical arms on which the force is applied? Because the four arms of the HJ meet at its center, we may recast the experimental configuration as a torque being applied around the central pivot point. The torque is proportional to the product of the magnitude of force and the distance between the point of application of the force and the pivot point (i.e., the length of the arm). Therefore, it could be expected that increasing arm length would result in a greater torque for the same force. We tested such a lever-arm effect using junction *XR*-long, where the X and R arms are lengthened by about a factor of two (from 11 bp to 21 bp) compared to junction *XR*. FRET histograms as a function of applied force (Fig. 1E and Fig. 1F) show that increasing the lever arm length has magnified the force effect such that much lower force is needed for junction *XR*-long to achieve the same conformational bias. Fig. S4 compares the transition rates versus the force between five molecules each of junctions *XR* and *XR*-long and shows that junction XR-long exhibits much greater changes in rates for the same magnitude of force (also compare $\Delta x_f^{\ddagger}$ and $\Delta x_b^{\ddagger}$ in Table 1). Because the persistence length of double-stranded DNA is about 50 nm (~150 bp) (*22*), the lever-arm effect can probably be extended by another factor of five for arms of ≥100 bp. That is, forces as low as 0.1 pN would be enough to influence the junction conformations, illustrating the exquisite force sensitivity of the HJ.

Because the effect of force depends on the arm lengths, the most natural reaction coordinates are angular. The angles that define the global shape of the junction are ϕ, the interhelical angle between two stacked pairs of helices, and ψ, the angle that measures the degree of unstacking of stacked helices (*23*) (Fig. 3B). For example, for a stacked-X structure, ϕ is 40° and ψ is 0° (*15*), whereas for an open structure, ϕ is 0° and ψ is 90° (Fig. 3C). These two angles are well-defined within the angular space in which identities of stacking pairs are maintained. Our aim is to deduce the structure of the transition state by determining the ϕ and ψ values of the transition state using a geometrical analysis. The analysis below estimates the angles (ϕ_{II}, ψ_{II}) of the transition state *ts*II in the *iso*II half of the conformational reaction coordinate, but the same conclusions hold for *ts*I.

*ts*II lies a third of the way from *iso*II to *iso*I along the d_{XR} coordinate (Table 1 and Fig. 3A). We can show that this condition is satisfied for a collection of (ϕ_{II}, ψ_{II}) values, starting from (70°, 0°) at one extreme and arriving at (0°, 70°) at the other (Fig. 3C, gray zone) (*18*). To obtain an additional constraint, we performed an equiv-

Table 1. Distance to the transition state from *iso*I ($\Delta x_f^{\ddagger}$) and from *iso*II ($\Delta x_b^{\ddagger}$), measured from the force-dependent transition rates between *iso*I and *iso*II for four different junctions. Errors represent SD from five different molecules each. Also shown is Δx_{eq}, the distance between *iso*I and *iso*II, determined from force-dependent changes in the equilibrium constant. For junction *BR*, Δx_{eq} deviates significantly from ($\Delta x_b^{\ddagger}$+$\Delta x_f^{\ddagger}$) showing that d_{BR} is not a valid reaction coordinate connecting *iso*I and *iso*II. In contrast, $\Delta x_{eq} = \Delta x_b^{\ddagger} + \Delta x_f^{\ddagger}$ within error for junctions *XR* and *HR*, showing that d_{XR} and d_{HR} are reaction coordinates valid from *iso*I to *iso*II.

	XR	XR-long	HR	BR
$\Delta x_b^{\ddagger}$ (nm)	1.5 (±0.3)	2.6 (±0.6)	2.4 (±0.5)	1.1 (±0.2)
$\Delta x_f^{\ddagger}$ (nm)	2.9 (±0.6)	7.7 (±1.5)	1.3 (±0.3)	0.37 (±0.2)
Δx_{eq} (nm)	4.4 (±0.8)	9.9 (±2.6)	3.1 (±0.8)	0.7 (±0.2)
$\Delta x_b^{\ddagger} + \Delta x_f^{\ddagger}$ (nm)	4.4 (±0.8)	10.3 (±2.0)	3.6 (±0.5)	1.5 (±0.3)

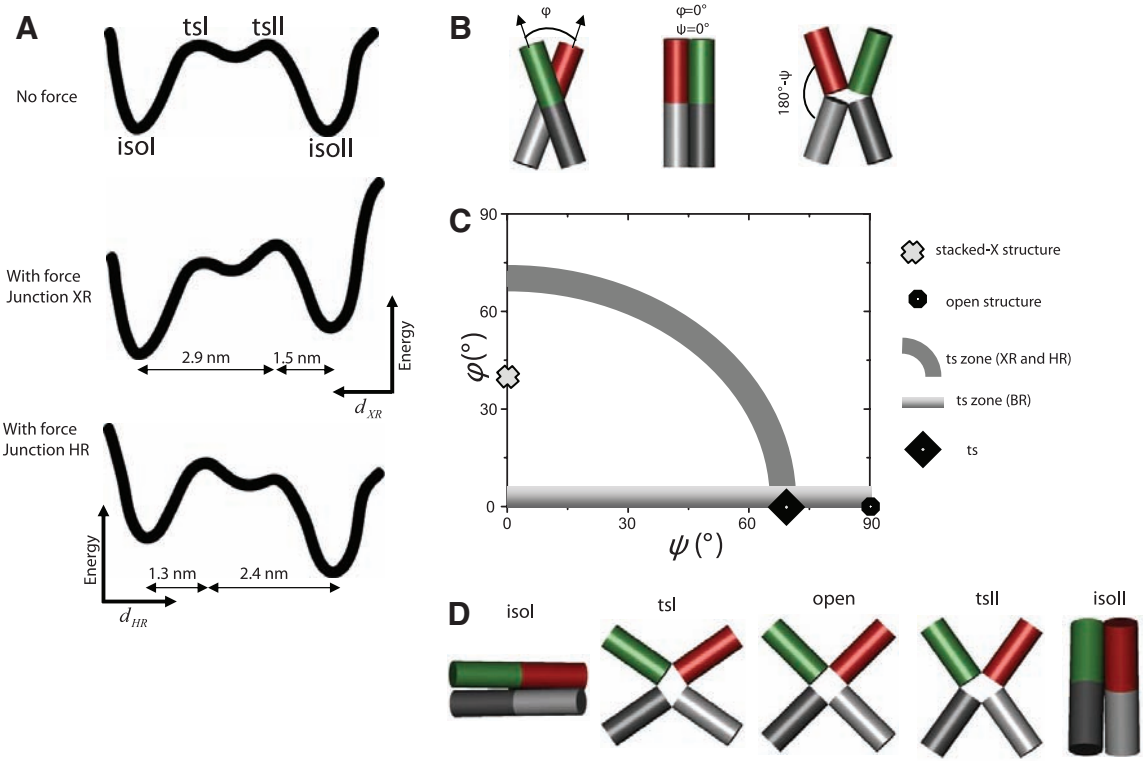

Fig. 3. Mapping the reaction landscape and determining the transition state structure. (**A**) A proposed reaction landscape with two distinct transition states with nearly identical energies (top). In junction *XR*, the applied force would tilt the energy landscape toward *isoI* so that the transition state, *ts*II, nearer to *iso*II would become the state of highest energy along the entire coordinate (middle). The reaction coordinate here is the distance between the ends of X and R arms, d_{XR}, which increases to the left as shown. Similarly, in junction *HR*, the transition state, *ts*I, nearer to *iso*I would become the single transition state upon application of force. The reaction coordinate here is the distance between the ends of H and R arms, d_{HR}, which increases to the right. (**B**) Two angular coordinates ϕ and ψ define the global conformation of the HJ. (**C**) A 2D conformational space of HJ conformations. The stacked-X structure and open structure are marked. The gray arc represents a zone that satisfies experimental constraints derived from *XR* and *HR* data, and the gradient zone is derived from *BR* data. The consensus location of the transition state is marked with a diamond. (**D**) Global structures of *iso*I, *iso*II, and two transition states, *ts*I and *ts*II, along with an open structure.

alent force analysis on junction *BR* (Fig. 2E, 2F, Table 1). Junction *BR* exhibited much reduced (by a factor of five or six) force dependence of the equilibrium populations compared with junctions *XR* and *HR* (compare Δx_{eq} values in Table 1). The residual force dependence of the equilibrium populations may be attributed to the finite diameter of the DNA duplex (*18*). In contrast to junctions *XR* and *HR*, application of force on junction *BR* accelerated both forward and backward transitions (Fig. 2F). Therefore, the distance between the ends of the B and R arms, d_{BR}, must be larger in the transition state than in the stacked-X structures. This condition is satisfied only if ϕ_{II} in the transition state is smaller than the 40° of the stacked-X structure. Furthermore, the distance to the transition state is 0.37 nm at minimum, which constrains ϕ_{II} to be essentially zero (*18*). In combination, our best estimate is $(\phi_{II}, \psi_{II})_{ts}$ = (0°, 70°) for *ts*II (Fig. 3C). This transition state is similar to the open state, but with arms deviating by about 20° from the ideal open state while displaying signatures on which pairs of helices are nearly stacked over each other (Fig. 3D). The structure bears a strong resemblance to the HJ structure bound to the Cre recombinase (*24*). Following the same argument, we can deduce that the transition state in the *iso*I-like conformational space, *ts*I, also has $(\phi_I, \psi_I)_{ts}$= (0°, 70°).

By probing the HJ dynamics in response to pulling forces in three different directions, we mapped the location of the transition states in the two-dimensional (2D) reaction landscape and deduced the global structure of the transient species populated during the HJ conformational changes. Our simplest model envisions a shallow minimum between the two transition states, depicted as the open structure (Fig. 3A and 3D), but it is also possible that a continuum of conformations exist, spanning from *ts*I and *ts*II with nearly identical free energies, instead of having a single well-defined minimum.

The development reported here expands on the current arsenal of hybrid single-molecule techniques combining force and other observables (*8*, *25*–*27*). Unlike DNA or RNA hairpins, where forces on the order of 15 pN are necessary to induce mechanical unzipping (*10*, *11*), the conformations of HJs could be biased at 0.5 pN or lower. The lever-arm effect makes it unlikely that a purely mechanical tool could have probed the force effect on HJ conformations, because if the arms are lengthened to magnify the distance change, the force effect will occur at even lower forces. FRET can also report on vectors other than the end-to-end distances, which we exploited here by pulling on *XR*, *HR*, or *BR* arms while simultaneously measuring the same HB vector by FRET, which led to the 2D mapping of reaction landscapes. Our method is readily applicable to other nucleic acids systems and their interaction with proteins and enzymes, and with the advent of new orthogonal labeling techniques, should be extendable to proteins and protein complexes. The next technical challenge would be to obtain time evolution of the end-to-end distance by force, for example, due to the action of DNA processing enzymes (*28*), and correlate it with the enzyme conformational changes simultaneously measured by fluorescence.

References and Notes

1. C. Bustamante, Y. R. Chemla, N. R. Forde, D. Izhaky, *Annu. Rev. Biochem.* **73**, 705 (2004).
2. L. Stryer, R. P. Haugland, *Proc. Natl. Acad. Sci. U.S.A.* **58**, 719 (1967).
3. T. Ha *et al.*, *Proc. Natl. Acad. Sci. U.S.A.* **93**, 6264 (1996).
4. T. Ha, *Methods* **25**, 78 (2001).
5. A. Ashkin, J. M. Dziedzic, J. E. Bjorkholm, S. Chu, *Opt. Lett.* **11**, 288 (1986).
6. A. N. Kapanidis *et al.*, *Science* **314**, 1144 (2006).
7. S. C. Blanchard, R. L. Gonzalez, H. D. Kim, S. Chu, J. D. Puglisi, *Nat. Struct. Mol. Biol.* **11**, 1008 (2004).
8. M. J. Lang, P. M. Fordyce, S. M. Block, *J. Biol.* **2**, 6 (2003).
9. P. B. Tarsa *et al.*, *Angew. Chem. Int. Ed. Engl.* **46**, 1999 (2007).
10. J. Liphardt, B. Onoa, S. B. Smith, I. Tinoco, C. Bustamante, *Science* **292**, 733 (2001).
11. M. T. Woodside *et al.*, *Science* **314**, 1001 (2006).
12. R. Holliday, *Genet. Res.* **5**, 282 (1964).
13. D. R. Duckett *et al.*, *Cell* **55**, 79 (1988).
14. D. M. J. Lilley, *Q. Rev. Biophys.* **33**, 109 (2000).
15. B. F. Eichman, J. M. Vargason, B. H. M. Mooers, P. S. Ho, *Proc. Natl. Acad. Sci. U.S.A.* **97**, 3971 (2000).
16. R. J. Grainger, A. I. H. Murchie, D. M. J. Lilley, *Biochemistry* **37**, 23 (1998).
17. Materials and methods are available as supporting material on *Science* Online.
18. S. A. McKinney, A. C. Declais, D. M. J. Lilley, T. Ha, *Nat. Struct. Biol.* **10**, 93 (2003).
19. J. C. Meiners, S. R. Quake, *Phys. Rev. Lett.* **84**, 5014 (2000).
20. I. Rasnik, S. A. McKinney, T. Ha, *Nat. Methods* **3**, 891 (2006).
21. S. A. McKinney, C. Joo, T. Ha, *Biophys. J.* **91**, 1941 (2006).
22. C. Bustamante, J. F. Marko, E. D. Siggia, S. Smith, *Science* **265**, 1599 (1994).
23. J. Yu, T. Ha, K. Schulten, *Nucleic Acids Res.* **32**, 6683 (2004).
24. G. D. Van Duyne, *Annu. Rev. Biophys. Biomol. Struct.* **30**, 87 (2001).
25. A. Ishijima *et al.*, *Cell* **92**, 161 (1998).
26. H. Shroff *et al.*, *Nano Lett.* **5**, 1509 (2005).
27. J. Gore *et al.*, *Nature* **439**, 100 (2006).
28. J. B. Lee *et al.*, *Nature* **439**, 621 (2006).

29. We thank W. Cheng at University of California–Berkeley for providing the protocol for the preparation of anti-Dig coated bead, M. Wang at Cornell University for giving generous advice about building optical tweezers, Y. Chemla at University of Illinois for helpful discussion, and C. Joo for generous help in preparation of illustrations. Funding was provided by the National Sciences Foundation CAREER Award (PHY 0134916) and the National Institutes of Health (GM065367). T.H. is an investigator with the Howard Hughes Medical Institute.

5 June 2007; accepted 11 September 2007
10.1126/science.1146113

A Metagenomic Survey of Microbes in Honey Bee Colony Collapse Disorder

Diana L. Cox-Foster,[1] Sean Conlan,[2] Edward C. Holmes,[3,4] Gustavo Palacios,[2] Jay D. Evans,[5] Nancy A. Moran,[6] Phenix-Lan Quan,[2] Thomas Briese,[2] Mady Hornig,[2] David M. Geiser,[7] Vince Martinson,[8] Dennis vanEngelsdorp,[1,9] Abby L. Kalkstein,[1] Andrew Drysdale,[2] Jeffrey Hui,[2] Junhui Zhai,[2] Liwang Cui,[1] Stephen K. Hutchison,[10] Jan Fredrik Simons,[10] Michael Egholm,[10] Jeffery S. Pettis,[5] W. Ian Lipkin[2]*

In colony collapse disorder (CCD), honey bee colonies inexplicably lose their workers. CCD has resulted in a loss of 50 to 90% of colonies in beekeeping operations across the United States. The observation that irradiated combs from affected colonies can be repopulated with naive bees suggests that infection may contribute to CCD. We used an unbiased metagenomic approach to survey microflora in CCD hives, normal hives, and imported royal jelly. Candidate pathogens were screened for significance of association with CCD by the examination of samples collected from several sites over a period of 3 years. One organism, Israeli acute paralysis virus of bees, was strongly correlated with CCD.

Methods for cloning nucleic acids of microbial pathogens directly from clinical and environmental specimens afford unprecedented opportunities for pathogen discovery and surveillance. Subtractive cloning, polymerase chain reaction (PCR), and DNA microarrays have implicated previously unknown pathogens as the etiological agents of several acute and chronic diseases. Here, we describe the application of unbiased high-throughput pyrosequencing technology (*1*) in the characterization of the microflora associated with *Apis mellifera* in a search for the cause of colony collapse disorder (CCD).

CCD is characterized by the rapid loss from a colony of its adult bee population (*2*–*4*). No dead adult bees are found inside or in close proximity to the colony. At the final stages of collapse, a queen is attended only by a few newly emerged adult bees. Collapsed colonies often have considerable capped brood and food reserves. The phenomenon of CCD was first reported in 2006;